Biology of Reproduction, 2017, 98(1), 63–74
doi:10.1093/biolre/iox155
Research Article
Advance Access Publication Date: 17 November 2017

OXFORD

Research Article

Distinct reorganization of collagen architecture in lipopolysaccharide-mediated premature cervical remodeling†

Shanmugasundaram Nallasamy[1], Meredith Akins[1], Breanna Tetreault[1], Kate Luby-Phelps[2] and Mala Mahendroo[1,*]

[1]Department of Obstetrics and Gynecology and Green Center for Reproductive Biology Sciences, University of Texas Southwestern Medical Center, Dallas, Texas, USA and [2]Department of Cell Biology, University of Texas Southwestern Medical Center, Dallas, Texas, USA

*__Correspondence:__ Department of Obstetrics and Gynecology and Green Center for Reproductive Biology Sciences, University of Texas Southwestern Medical Center, 5323 Harry Hines Blvd, Room F2.306, Dallas, TX 75235-9032, USA. Tel: +214-6483091; E-mail: mala.mahendroo@utsouthwestern.edu

†__Grant Support:__ This work is supported by National Institutes of Health HD043154 (MM), March of Dimes #21-FY2014-131 (MM), and National Institutes of Health S10 OD020103-01 (KLP).
Edited by Dr. Peter J. Hansen, PhD, University of Florida.

Received 30 August 2017; Revised 10 November 2017; Accepted 16 November 2017

Abstract

Previous work has identified divergent mechanisms by which cervical remodeling is achieved in preterm birth (PTB) induced by hormone withdrawal (mifepristone) or lipopolysaccharide (LPS). Our current study aims to document how collagen architecture is modified to achieve premature cervical remodeling in mice treated with LPS as a model of infection-induced inflammation. Cervices were collected on gestation day (d) 15 from mice with premature cervical ripening induced by LPS and compared to d15 and d18 controls as well as a hormone withdrawal PTB model. Second harmonic generation (SHG) and electron microscopy were utilized for visualization of collagen morphology and ultrastructure. LPS-mediated premature cervical ripening is characterized by unique structural changes in collagen fiber morphology. LPS treatment increased the interfibrillar spacing of collagen fibrils. A preferential disruption of collagen fiber architecture in the subepithelial region compared to midstroma region was evidenced by increased pores lacking collagen signal in SHG images in the LPS-treated mice. Coinciding with this alteration, the infiltration of neutrophils was concentrated in the subepithelial stromal region as compared to midstromal region implicating the potential role of immune cells to extracellular matrix reorganization in inflammation-induced preterm cervical ripening. The current study demonstrates a preferential disorganization of collagen interfibrillar spacing and collagen fiber structure in LPS-mediated ripening.

Summary Sentence

Region specific reorganization of cervical collagen structure in LPS-induced preterm birth.

Key words: preterm birth, cervix, collagen.

Introduction

Preterm birth (PTB) affects 1 in every 10 babies in the United States [1]. Elucidating the exact mechanisms of PTB is critical to reduce the rates of infant mortality and lifelong health complications associated with prematurity [2, 3]. It is complicated by the fact that risk factors and etiologies are numerous and many remain unidentified [4, 5]. Furthermore, the molecular mechanisms that govern key aspects of the PTB process differ from physiologic term parturition [6–8].

Irrespective of etiology, cervical changes precede the onset of term or PTB, thus investigations to understand these early cervical changes may provide insights to improve clinical outcomes [9, 10]. Investigations in mouse models of PTB have provided key insights into these distinct processes [9, 11–13]. Two accepted paradigms of PTB are infection and functional progesterone loss [7, 14]. To mimic these pathways in mice, an "infection model" is applied in which lipopolysaccharide (LPS) is administered directly into the uterus for a localized intrauterine infection (IU-LPS). To mimic progesterone loss ("noninfection" model), the progesterone receptor antagonist, mifepristone, is administered by subcutaneous injection [15]. The resulting premature loss of progesterone function most closely mimics parturition at term [7, 16]. Both the infection and noninfection model result in murine PTB.

The collective findings of studies in mice treated with IU-LPS reveal unique gene/protein expression patterns and immune cell populations in the preterm cervix and myometrium that are distinct from patterns at term [7, 17]. In the cervix, these include increased proinflammatory genes/proteins (e.g., interleukin 6, interleukin 1 alpha, tumor necrosis factor alpha), increased numbers of activated neutrophils/macrophages, and increased cervical prostaglandin-endoperoxide synthase 2 (PTGS2) expression and prostaglandin levels. Prostaglandins are critical for LPS-mediated premature ripening as PTGS2 inhibition can reduce rates of LPS-induced premature ripening but not term ripening [18]. In addition, cervical wet weight and plasma estradiol levels fail to increase as they do at term. Genes normally induced during cervical ripening at term such as the oxytocin receptor, connexin 26, and hyaluronan synthase 2 as well as genes associated with epithelial cell differentiation are not upregulated in LPS-mediated cervical ripening [7]. Despite the marked differences between LPS-mediated premature ripening and term cervical ripening, tissue compliance increases to a similar extent as determined by biomechanical testing. This suggests that reorganization of the extracellular matrix (ECM) is achieved in both pathways [18].

The cervix is a dense connective tissue consisting of a rich ECM [19, 20]. Cells within the cervical stroma include both fibroblasts and smooth muscle cells, which are responsible for the synthesis of an ECM that changes in composition and structure in response to physiological signals [21]. Remodeling of ECM is essential to successful birth [10, 22]. Tissue mechanical strength is influenced by the abundance, cross-link density, and structural organization of fibrillar collagen as well as changes in the composition of noncollagen ECM molecules [23–26]. During normal pregnancy, cervical collagen undergoes a progressive change in collagen cross-link density and structural organization with no decline in collagen content [24, 25]. However, current literature regarding collagen content in premature cervical ripening varies between studies and little is known of the structural organization of collagen in these models. Studies looking at the effects of mifepristone on human cervix, following first trimester abortions as well as murine cervix, showed no change in collagen content [27]. In contrast, studies in the mifepristone-treated rat report a reduction on collagen content [28, 29]. Few studies correlate changes in collagen with LPS treatment. However, one study reports a decline in collagen content in LPS-treated rabbits as assessed by picrosirius red staining [30]. Holt et al. report constant collagen levels post-LPS or mifepristone treatment in mice using the hydroxyproline assay to determine collagen content [7].

Clarification of the specific molecular pathways that drive infection-mediated premature cervical ripening is required to identify clinically relevant targets for early detection of risk and for prevention of subsequent premature birth. With this goal in mind, the focus of this study is to understand how cervical collagen structure and organization is altered during premature cervical ripening induced by inflammation to allow changes in the biomechanical function of the cervical tissue. These investigations will compare LPS-induced ripening as a model of infection-mediated ripening to term ripening and when relevant also compare to a noninfection model of premature birth.

Materials and methods

Animals

Mice used for these studies were of C57B6/129Sv mixed strain and were maintained in a barrier facility. Mice were housed under a 12 h-light/12 h-dark cycle at 22°C. Nulliparous mice between the ages of 2–6 months were used in this study. The day of vaginal plug was considered as day 0 of pregnancy. Studies were conducted in accordance with the standards of humane animal care described in the National Institutes of Health Guide for the Care and Use of Laboratory Animals using protocols approved by the University of Texas Southwestern Medical Center animal care and research advisory committee.

Mifepristone treatment

Premature labor was induced on gestation d15 by administration of the progesterone receptor antagonist, mifepristone as described previously [7]. Mifepristone was solubilized in ethanol and brought up in glyceryl trioleate (Sigma, St. Louis, MO). Mice were given 0.5 mg of mifepristone (Sigma) in glyceryl trioleate (Sigma) or vehicle control (50 μl ethanol + 150 μl glyceryl trioleate) by subcutaneous injection at 21:00–22:00 hours late on the evening of gestation day 14. Mice were sacrificed and cervices collected 12 h after on gestation day 15. Administration of the progesterone receptor antagonist, mifepristone, results in premature cervical ripening and PTB 13–16 h after injection [15, 28].

Lipopolysaccharide treatment

To ensure initiation of PTB at a similar time point in gestation as the mifepristone model, LPS was administered early on gestation day 15 (approximately 8 am) and cervices collected at midday on d15 as described previously [7]. Briefly, mice were anesthetized using isoflurane on the early morning of gestation day 15. Using sterile surgical practices, a small incision was made in the ventral abdomen to expose the uterus. Once uterus was visualized, 150 μg of LPS (O55:B5, Sigma) dissolved in 30 μl of sterile water was injected into the uterus in between two fetal sacs with care to avoid fetal membranes. The skin was closed with wound clips. After surgery, 0.1 μg/kg buprenorphine (Hospira, Lake Forest, IL) was given for pain management. Mice were sacrificed and cervices collected 6 h postsurgery. The sham group was injected with 30 μl of sterile water through the same procedure. Administration of intrauterine LPS results in preterm delivery approximately 7–8 h postinjection [7].

RNA isolation and quantitative PCR

Total RNA was extracted using RNA Stat-60 (Tel-test B, Friendswood, TX) according to the manufacturer's protocol and treated with DNase-I (Ambion, Austin, TX) to remove genomic DNA. Complementary DNA was prepared using iScript Reverse

Transcription Supermix (BioRad, Hercules, CA). Quantitative PCR (qPCR) was performed using SYBR Green and a PRISM 7900HT sequence detection system (Applied Biosystems). Gene expression was calculated according to the 2–ΔΔCt method as described (User Bulletin no. 2; Applied Biosystems). The target gene expression was normalized to the expression of the housekeeping gene, cyclophilin B (Ppib). The Grubbs statistical test was performed to determine the significant outliers that were appropriate to remove from the final analysis. Five to eight cervices were used for each time point or treatment group.

Dot blot

Collagen was extracted with 7 M urea (Sigma), 0.1 M sodium phosphate with 1% protease inhibitor (Sigma), overnight at 4°C (n = 3 cervices per time point or treatment group). This included gestation d15, d18, d15-LPS sham, d15-LPS, d15-MFP sham, and d15-MFP. The protein concentration was determined by a Bradford protein assay (Pierce, Thermo Scientific, Rockford, IL). Protein (2.5 μg) was spotted onto a nitrocellulose membrane and probed with a rabbit polyclonal anticollagen I or rabbit polyclonal anticollagen III primary antibody (Abcam, Cambridge, ab34710 and ab7778) (Supplementary table 1). Secondary antibody for both western and dot blots was donkey antirabbit HRP (Jackson ImmunoResearch, Pennsylvania, #711036152). Chemiluminescence was visualized using ECL (GE Healthcare, Buchinghamshire, UK). Digital images of the blots were analyzed quantitatively using Multi Gauge software (Fuji Film, Tokyo).

Immunofluorescence of collagen

Cervical tissue was collected at 12 h postinjection of mifepristone and 6 h postinjection of LPS and frozen in OCT medium (Tissue Tek, Indiana). This included gestation d15, d18, d15-LPS sham, d15-LPS, d15-MFP sham, and d15-MFP. Eight-micrometer cervical cross-sections were cut from tissue blocks. Sections were fixed for 10 min in acetone at –20°C. Tissue was rehydrated in PBS, blocked in 10% normal goat serum (Invitrogen, California, catalog # 01-6201), and incubated with collagen I or collagen III rabbit polyclonal antibodies (Abcam, Cambridge, ab34710 and ab7778). Sections were then washed in PBS and incubated with goat α rabbit IgG antibodies coupled to Alexa 488 (Invitrogen/Molecular Probes, California, A11008). Slides were viewed on a Zeiss LSM510 META NLO confocal microscope using an Acroplan 40x/0.8 W objective lens. Fluorescence signal intensity was measured using ImageJ 1.41k (http://rsbweb.nih.gov/ij/) (n = 3 animals per time point/12 images per time point). Four images were taken in the midstroma region of the cervical cross-section from each animal. A schematic indicating regions defined as midstroma and subepithelial stroma for studies in this paper is in Supplementary Figure S1.

Scanning electron microscopy

Scanning electron microscope (SEM) images were obtained from gestation days 15 and 18 for comparison to LPS-treated mice on gestation day 15. Mice were perfused with 1% glutaraldehyde, 2% paraformaldehyde in 0.1 M phosphate buffer. Cervices were dissected from uterine and vaginal tissues and were fixed with 2.5% (v/v) glutaraldehyde in 0.1 M sodium cacodylate buffer overnight at 4°C. After three rinses in 0.1 M sodium cacodylate buffer, they were postfixed with 2% osmium tetroxide in 0.1 M sodium cacodylate buffer with 0.1% ruthenium red for 2 h. Samples were rinsed with water and dehydrated with increasing concentration of ethanol, followed by increasing concentrations of Hexamethyldisilazane in ethanol. Tissue samples were air dried under the hood, mounted on SEM stubs and sputter coated with gold/palladium in a Cressington 108 auto sputter coater. Images were acquired on a Field-Emission Scanning Electron Microscope (Zeiss Sigma) at 2 kV accelerating voltage. As indicated in Supplementary Figure S2, low magnification allowed identification of the midstroma (MS) region which was subsequently imaged at 200 000× as seen in Figure 4 (n = 3–4 animals per time point).

Transmission electron microscopy

Cervical tissue was collected, processed, and imaged as described previously [24]. This included gestation d15, d18, d15-LPS sham, d15-LPS, and d15-MFP (n = 3 animals per time point with approximately 20 images taken from each group). Briefly, mice were perfused with 1% glutaraldehyde, 2% paraformaldehyde in 0.1M phosphate buffer. Cervical and uterine tissue was removed and fixed in 2.5% glutaraldehyde in 0.1 M cacodylate buffer containing 0.1% ruthenium red overnight at 4°C. Vaginal and uterine tissue was removed from the cervix and the cervix was rinsed for 30 min with cacodylate buffer. The tissue was postfixed with 1% osmium in 0.1 M cacodylate buffer containing 0.1% ruthenium red for 90 min. Specimens were dehydrated through a graded series of ethanol (50%, 70%, 95%, 100%) followed by propylene oxide and embedded in Epon. Thin sections were stained with uranyl acetate and lead citrate. Sections were viewed on a Tecnai Spirit Biotwin transmission electron microscope (FEI Company, Hillsboro, Oregon) and images captured at 4200× or 20 500× with a Morada 11 megapixel CCD camera.

Collagen fibril measurements

Collagen fibril diameter was compared between gestation d15-sham and d15-LPS-treated groups as described previously [24]. Briefly, electron microscope images of collagen fibrils taken at 20 500× were analyzed with Image J 1.41k (http://rsb.info.nih.gov/ij/). An intensity threshold was interactively determined for optimal segmentation of fibril from background. Segmented images were converted to a binary mask, and erode, open, dilation and fill holes binary operations were used to separate merged fibrils. Particles were analyzed using the Particle Analysis function of Image J with parameters set for size, 1000–10 000 and circularity 0–1. Ellipses were fit to all particles and the minor angle of the ellipse was taken as the fibril diameter.

Interfibrillar spacing measurements

Electron microscopy images taken at 20 500× were used to assess interfibrillar spacing. The images were superimposed on an 8 × 6 grid overlay by using the Analyze>Tools>Grid function of the ImageJ program. Collagen fibrils within a single collagen fiber bundle filled each grid and the number of fibrils present within each square was counted using cell counter in ImageJ. A total of 216 squares were counted manually per time point/treatment. The frequency distribution histogram was generated for squares based on the number of fibrils present per square. In this experiment, images were taken from the cervix of three to four animals of gestation day 15, day 15 sham, and day 15 with IU-LPS treatment. The collagen fibril diameter was constant between these three groups. The day 18 cervices were not included in this experiment because the collagen fibril diameter significantly increases on day 18 compared to day 15 cervices [24].

Second harmonic generation imaging and image analysis

Second harmonic generation (SHG) imaging and image analysis were performed as described [31]. Images were obtained from the MS and subepithelial (SE) stroma of each tissue section (see Supplementary Figure S1). Time points and treatment groups included gestation d15, d18, d15-LPS sham, d15-LPS, and d15-MFP (n = 3 animals per time point with approximately three to four images taken from each sample/region). Briefly, cervices were snap frozen at liquid nitrogen temperature in OCT (Tissue Tek, Indiana) and were cut into 50 μm cross-sections. Sections were mounted on glass slides under #1.5 glass coverslips (Corning, Corning, NY). Frozen sections were thawed and covered in 0.1 M PBS to maintain hydration during imaging on a Zeiss LSM510 META NLO configured with an Axiovert 200M inverted microscope and using an Achroplan 40×/0.8 W objective lens. A Chameleon XR pulsed Ti:sapphire laser (Coherent, California) tuned to 900 nm was focused onto the stroma of the cervix and the resulting SHG signal was detected at 450 nm. Forward scattered signal was detected with the transmitted light detector of the microscope after excitation light was removed by a HQ 450 sp-2p filter (Chroma Technology, Vermont). Backward scattered signal was detected with a nondescanned detector placed at the illumination port of the wide-field epifluorescence light path. Backscattered excitation light was removed using a 680 nm short-pass dichroic mirror. Images were analyzed using ImageJ 1.41k (http://rsbweb.nih.gov/ij/), to quantify image intensity, fiber diameter, and porosity as described previously [31].

Dual imaging for neutrophils and fibril collagen by immunofluorescence and second harmonic generation respectively

Eight micrometer (frozen) sections were prepared for immunofluorescence (IF) using neutrophil/monocyte 7/4 antibody (Serotec, Raleigh, NC). Using a Zeiss 510 LSM microscope, 225 × 225 μm tiled images of forward and backward SHG together with IF were taken with the 40× objective (day 15 n = 3, d15-LPS Sham n = 2, and d15-LPS n = 5). Channel settings were initially set based on the LPS-treated tissues and were kept the same for all image acquisitions. The number and size of extravascular positive regions presumably representing clusters/swarms of neutrophils was analyzed using ImageJ. A threshold intensity was chosen to create a binary mask of the IF signal above background within the area of the cervical stroma and the particle analysis function was used to obtain the number and size of positive particles under the mask using a lower size cutoff to exclude noise. These data were used to determine the area fraction of neutrophils in the field of view as well as the mean cluster size.

Statistics

Statistics were performed using Prism software version 5.0b (Graph Pad Software, La Jolla, CA). For comparison of qPCR, collagen content, fibril diameter data, porosity measurements and neutrophil cluster size, one-way ANOVA was used. Values are expressed as mean ± SEM. P value < 0.05 was considered significant.

Results

Assessment of fibrillar collagens I and III and factors involved in their processing and assembly

We evaluated expression of genes encoding collagens I and III (*Col1a* and *Col3a*), enzymes required for collagen cross-link formation, lysyl oxidase and lysyl hydroxylase 2 (*Lox* and *Plod2*), and matricellular proteins whose expression is constant (secreted protein acidic and cysteine rich, *Sparc*) or downregulated in the pregnant cervix (tenascin C (*Tnc*) and thrombospondin (*Thbs*) 1 and 2) (Figure 1). Relative to gestation day 15 controls, collagen 1 and 3 expression was not changed during LPS-mediated ripening. There was a significant increase in transcripts encoding the cross-link forming enzyme, *Lox*. While mRNA expression encoding the matricellular protein *Sparc* was not altered, expression of both *Tnc, Thbs* 1 and 2 was markedly increased in the LPS group as compared to day 15 untreated control cervices. We next examined possible changes in the relative abundance of the major and minor fibrillar collagens in the cervix, collagen I and III, respectively, by dot blot and IF analysis. Dot blot assessment of total protein was performed (Figure 2). Conventional western immunoblotting could not be used for this assay because the antibodies specific for collagen type III do not recognize denatured protein. Mature collagen with heavy cross-links has poor solubility in 7 M urea. A decline in cross-links or change in processing of collagen can alter its solubility allowing the collagen to be more readily extracted in 7 M urea. Blots showed equal amount of collagen for all treatment groups and time points, indicating that changes in collagen properties in the two PTB models does not affect the ratio of collagen I to III (Figure 2).

Collagen III is known to influence collagen I fibrillogenesis. Tissue strength can differ with changes in the ratio of collagen I/III [32–34]. As an additional approach to assess potential changes in the collagen I to III ratio, collagen I and collagen III IF was performed. This technique will estimate the total population of collagen in contrast to protein dot blots, which provide an estimate of collagen that is extractable in 7M urea. Representative intensity matched-IF images of collagen I are shown in panel 3A and the IF intensity ratio of collagen I to collagen III (images not shown) is depicted in Figure 3B. The collagen I/III ratio was approximately 2.0 for all treatment groups and gestation days. This suggests that there is no difference in the relative abundance or ratio of collagen I to III in the cervices from LPS- or mifepristone-treated mice as compared to the gestation-matched time point (day 15) and term ripening (gestation day 18). Interestingly, collagen I fluorescence images reveal marked differences in collagen structure between the LPS treatment group compared with both the mifepristone treatment group and with normal gestation. During normal gestation between day 15 and day 18, there is a change in the pattern of collagen I staining. Increased spacing is apparent between the regions that stain for collagen I in the normal day 18 cervices. Mifepristone-treated cervices show an even greater increase in spacing between collagen I signal than what is seen on gestation day 18. This observation is consistent with our previous SHG images of MFP-treated cervices [31]. However, the collagen staining of LPS-treated cervices remains indistinguishable from the day 15 cervices (Figure 3).

Extracellular matrix and collagen ultrastructure

As described above, neither a decline in collagen synthesis, change in ratio of collagen type I to III, or a change in the morphology of collagen I staining as observed in IF images provide insight into potential mechanisms by which collagen reorganization reduces the mechanical strength of the cervix in LPS-mediated cervical ripening. In the next series of studies, scanning and transmission electron microscopy were utilized to observe collagen and ECM ultrastructure in the cervix of mice treated with LPS. Scanning electron micrographs from gestation day 15, day 18, and day 15-LPS treated

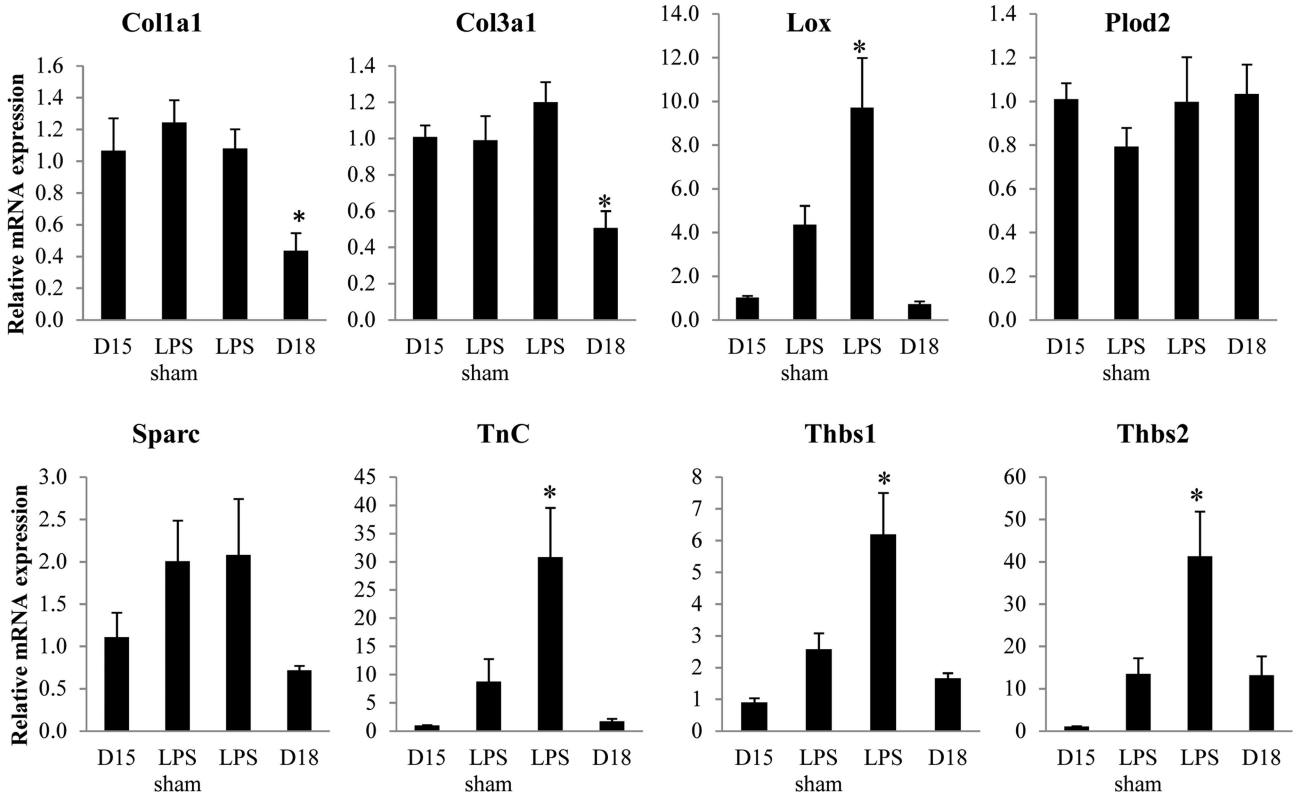

Figure 1. mRNA expression of collagen and factors involved in fibrillogenesis. Messenger RNA expression of genes encoding collagens I and III (*Col1a* and *Col3a*), enzymes required for collagen cross-link formation (*Lox* and *Plod2*), and matricellular proteins (*Sparc, Tnc,* and *Thbs* 1, 2) were evaluated in gestation day 15, day 15 sham, day 15 IU-LPS, and day 18 cervix. Data represent the average of five to eight cervices for each time point or treatment ±SEM (*$P \leq 0.05$).

were compared (Figure 4). No clear difference in the morphology of collagen fibrils, their organization into fibers, or the overall architecture of the collagen matrix was evident. Transmission electron micrographs from gestation day 15, day 18, day 15- mifepristone treated and d15- LPS treated were compared (Figure 5A). As evident in the low-magnification images, the density of collagen fibrils in the LPS-treated group was similar to d15 and d15-sham surgery groups. In contrast, collagen fibrils in mifepristone-treated cervices appear markedly more dispersed with large empty spaces between fibers even more dramatic than at term ripening on d18 of normal gestation. As previously reported, collagen fibril diameter increased from gestation day 15 to day 18 in normal pregnancy [24]. As seen in Figure 5B, collagen fibril diameter measurements in LPS-treated cervices (63.4 nm) were similar to day 15 sham (61.4 nm). Collagen fibril diameters in the cervices of mifepristone-treated mice were not quantified due to the technical difficulty in measuring the markedly dispersed fibrils. A second quantifiable feature of collagen fibrils is the spacing between fibrils. The interfibrillar spacing in LPS-treated cervices was increased somewhat compared to gestation day 15 and day 15 sham cervices (Figure 5A). There is an overall shift to the left for the average number of fibrils per square in day 15-LPS-treated cervices compared to day 15 and sham control cervices, which suggests increased spacing between fibrils (Figure 5C). MFP-treated collagen fibrils were unable to be analyzed for fibril diameter and interfibrillar spacing due to the increased amount of dispersion seen in TEM micrographs.

Collagen I second harmonic generation in preterm birth models

Forward SHG microscopy of cervical frozen sections was performed to assess region-specific structural changes in collagen I fibers in PTB models and term ripening (Figure 6). Our previous studies in the mouse cervix and numerous other studies demonstrate the utility of quantifying features of collagen in SHG images to assess structural changes in collagen organization [31, 35, 36]. Our previous studies quantifying cervical collagen fiber diameter and porosity in SHG images were evaluated in the cervical midstroma [31]. In the current study, images were obtained from cervical cross-sections in the MS and SE regions (Figure 6A). Consistent with our previous findings in the MS, the images of mifepristone-treated cervices showed an increase in the number and size of regions lacking SHG signal (pores in the collagen matrix) relative to untreated day 15 in both the MS and SE regions of the cervix (Figure 6A). In contrast, an increase in pore size was apparent only in the SE stromal region in the d15-LPS-treated group as well as d18 term group (Figure 6A). To quantify this apparent difference, the area, size, spacing, and number of pores were evaluated as described [31]. The pore % fractional area and the average pore size were significantly higher in mifepristone-treated groups compared to all other groups in both the SE and MS regions (Figure 6B). In the d15-LPS-treated group, pore area % and pore size increased in the SE stroma relative to d15 but not the MS (Figure 6B). There were no differences in pore spacing and pores per unit area for either PTB model. These results identify distinct regional differences in structural reorganization of collagen fibers between term and PTB

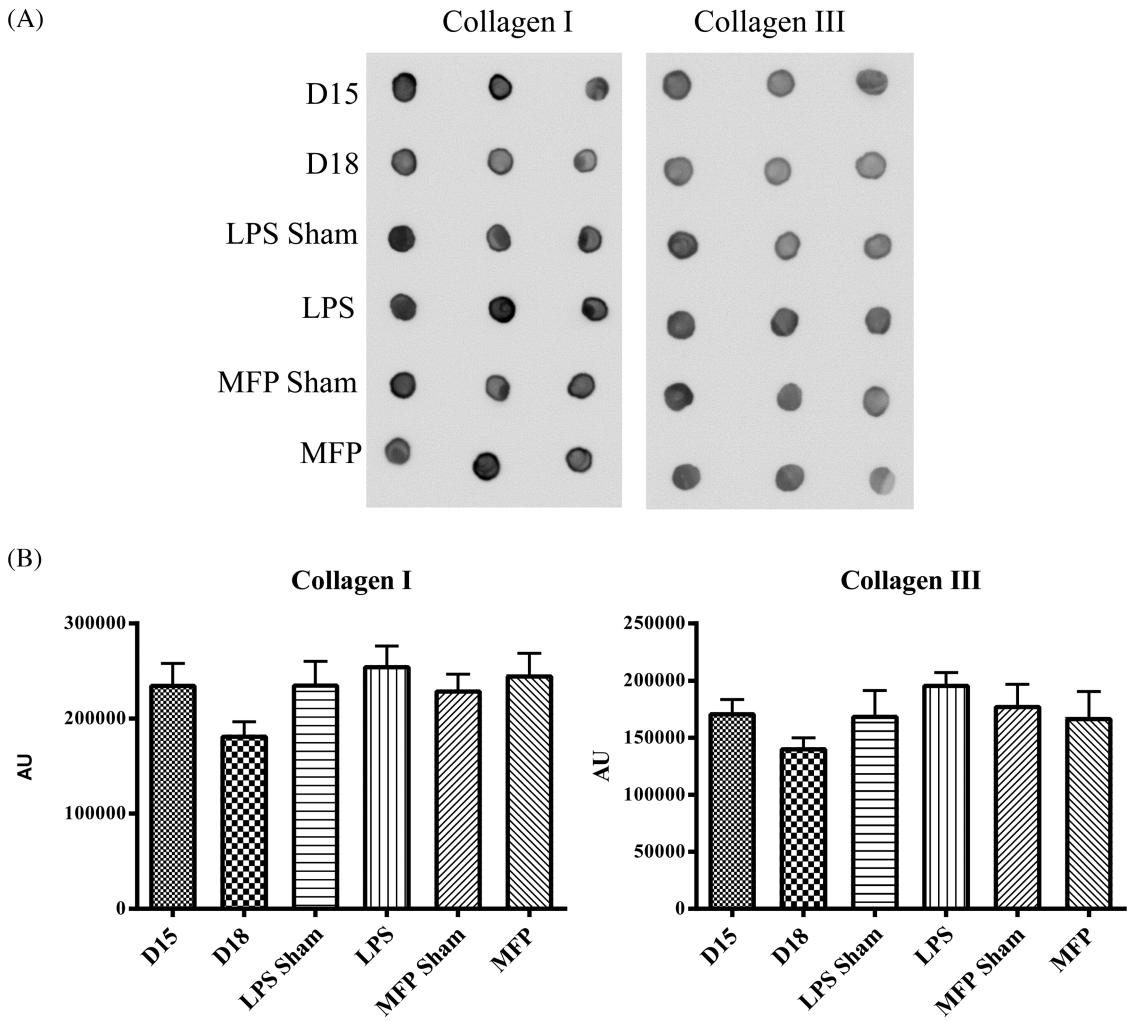

Figure 2. Cervical collagen I and III levels remain constant in PTB models. (A) Dot blot analysis of collagen I and collagen III protein levels in gestation day 15, day 15 sham surgery, day 15 LPS, MFP sham, d15 MFP and gestational day 18 cervix. (B) Optical density analysis of collagen I and III dot blot. n = 3 cervices per time point.

models. Specifically, pore area and size are increased in the SE stroma of both preterm models and term, while an increase in pore area and size in the MS was only observed in the mifepristone-treated mouse.

Role of neutrophils in regional collagen remodeling during lipopolysaccharide-mediated ripening

The collagen SHG data clearly identify structural changes of collagen I fiber organization in LPS-treated cervices predominantly in SE stromal regions. While SHG data in the day 18 SE stroma of gestation day 18 mice also indicate a structural reorganization, the mechanism of reorganization may be distinct due to macrophage and neutrophil-mediated secretion of collagenases in response to LPS administration. This hypothesis is supported by the marked increase in macrophages and neutrophils and expression of the neutrophil-localized collagenase, MMP8 in LPS-mediated ripening [7]. Previous studies in other tissues report the formation of cluster or swarms of activated neutrophils migrated from nearby interstitial tissue as well as from blood vessels that are able to displace or clip collagen leading to the collagen-free zones [37]. To see whether regional clipping or disorganization of collagen near tissue neutrophils might be responsible for the reorganization of SE collagen I in the LPS model of PTB, we combined SHG imaging with IF localization of neutrophils using the antibody 7/4 which recognizes both neutrophils and monocytes. As the boundaries of blood vessels were evident in the SHG images, we preferentially selected neutrophil clusters that were not in blood vessels. As seen in Figure 7A, neutrophils/neutrophil clusters indicated by red IF were notably increased in number and size in the cervical stroma of the LPS group as compared to untreated and sham controls. Additionally, these neutrophil clusters are concentrated in the SE stromal region compared to midstromal region. The IF signal in the cervical SE stroma and MS was quantified to assess cluster size and fractional area occupied by neutrophils (Figure 7B). Both cluster size and percent area occupied were significantly increased in the LPS-treated and sham group as compared to day 15. A modest increase in cluster size and fractional area was observed in the sham-operated group but was primarily localized to the endocervical epithelia in contrast to the SE and MS accumulation of neutrophils following LPS treatment. The SHG channel revealed that collagen I signal was largely absent from neutrophil positive areas in the cervices of LPS-treated mice as shown in Figure 7C.

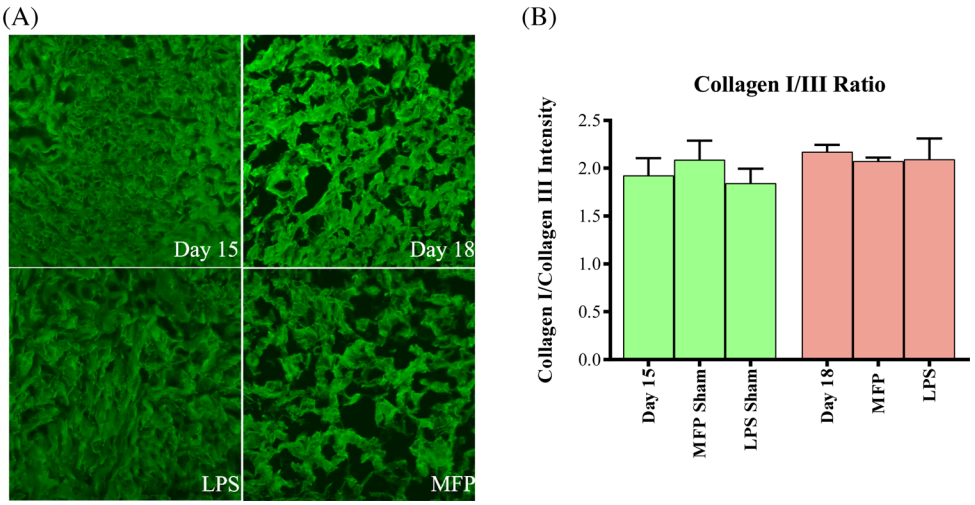

Figure 3. Collagen I/III ratio remains unaltered in PTB models. (**A**) Immunofluorescence of collagen I in gestation day 15, gestation day 18, day 15 LPS-treated and mifepristone-treated cervices reveals cervical collagen structure. (**B**) Immunofluorescence intensity of collagen I and collagen III was measured and collagen I/III ratio was determined for gestation day 15, day 18, day 15 LPS and mifepristone treatment, and LPS and mifepristone sham treatments. Ratio of collagen I/III was approximately 2.0 for all time points and treatments. Error bars represent standard error mean. n = 3 animals per time point/12 images per time point.

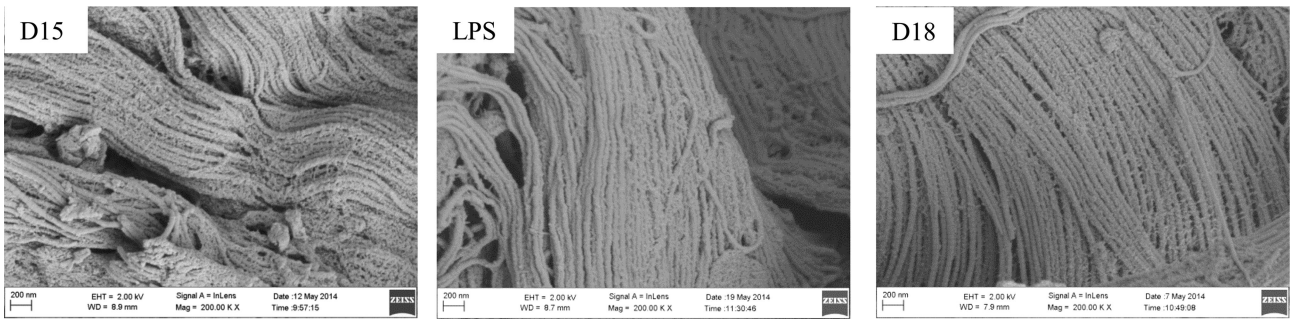

Figure 4. Scanning electron micrograph imaging exhibits no structural change in collagen fibrils. Scanning electron micrographs of cervical ECM taken on gestation day 15, day 15 LPS treatment, and gestation day 18. Magnification: 200 000×. Bar = 200 nm. n = 3–4 animals per time point.

Discussion

The mechanical load-bearing properties of the cervix arise primarily from three-dimensional architecture of collagen fibers [23, 38]. Through pregnancy, a sequence of steroid hormone-regulated changes in the turnover, processing, and assembly of collagen fibrils are key determinants in orchestrating a gradual alteration in cervical mechanical function [9, 39]. For the majority of pregnancy, the cervix undergoes gradual softening—a period in which tissue competence is balanced with a gradual increase in compliance [40]. Near term, the cervix transitions to the ripening phase in which competence is lost and compliance is maximal. Studies in mice have established that induction of premature birth on gestation day 15 by LPS-mediated inflammation or mifepristone-mediated blockage of progesterone function is preceded by premature mechanical ripening of the cervix with a similar decline in tissue stiffness as reported at term [18]. The molecular pathway, by which LPS-mediated premature ripening is achieved, however, is markedly distinct from term and mifepristone-mediated preterm ripening. The most notable difference is the robust proinflammatory response, prostaglandin dependence, and the achievement of maximal tissue compliance without a parallel increase in the estrogen to progesterone ratio. We thus anticipated differences in collagen structure with LPS-mediated ripening compared with normal gestation and in the current study we sought to understand how the structural reorganization of collagen architecture is achieved in the unique setting of LPS-mediated premature ripening.

Synthesis of collagen fibrils appeared normal in cervices from LPS-treated mice, as we did not find a change in the ratio of fibrillar collagen I and III or a decline in expression of genes encoding fibrillar collagens. Assessment of collagen structure by light and electron microscopy however provided insights into distinct processes by which loss of cervical compliance is achieved in the LPS PTB model. In mifepristone-treated mice, the assessment of collagen fibril ultrastructure by TEM revealed a dramatic change in collagen organization that was similar though more pronounced as compared to term ripening. This observation was consistent with the previous findings that in this mouse model of PTB immune cell influx, gene expression patterns and steroid hormone profiles were similar to term ripening or shortly postpartum [7, 16]. In contrast, collagen fibrillar ultrastructure in cervices from LPS-treated mice was similar to untreated- or sham surgery-d15 controls and collagen fibers did not appear dramatically reorganized unlike in the mifepristone treated and term ripening. Though the diameter of the fibrils was similar to gestation day 15, we did observe a subtle but significant alteration in interfibrillar spacing. The interfibrillar spacing is regulated by interfibrillar bridges which are formed and maintained by proteoglycans such as

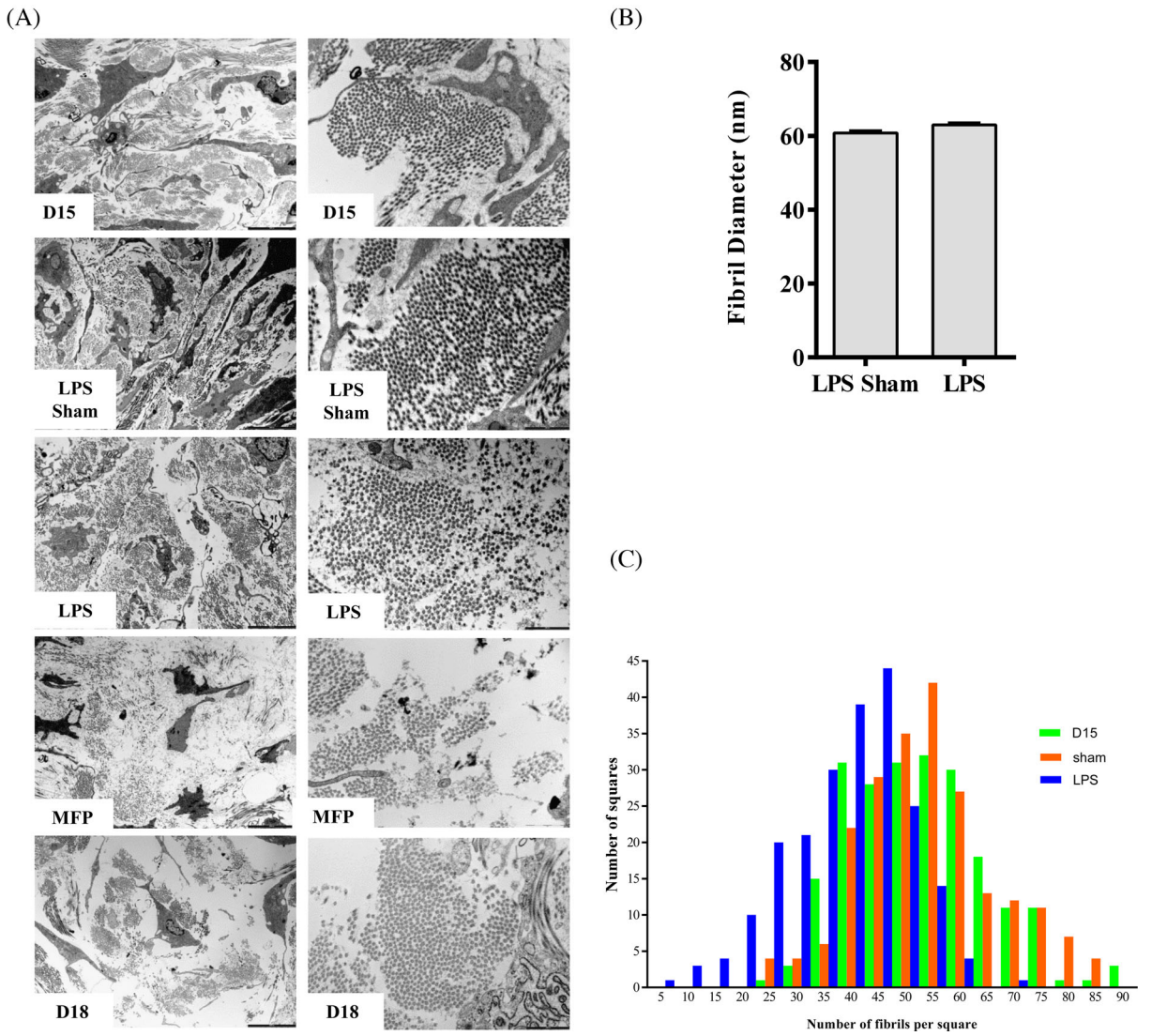

Figure 5. Ultrastructural assessment of cervical collagen fibril organization, diameter, and spacing. (A) Transmission electron micrographs of cervical ECM taken on gestation day 15, day 15 sham, day 15 LPS, and mifepristone treatment and day 18. Left panel: 4200×; right panel: 20 500× magnification. (B) Collagen fibril diameter is not altered in the LPS-treated cervix. Electron micrographs taken at 20 500× of cervical sections from gestation day 15 sham treated and day 15 LPS-treated mice. Collagen fibrils were analyzed for fibril diameter. LPS treatment does not cause an increase in collagen fibril diameter. n = 2922 fibrils for sham treatment and n = 4231 fibrils for LPS treated. n = 3 animals per treatment group. (C) Interfibrillar spacing of collagen fibrils is increased in response to LPS treatment. Electron micrographs taken at 20 500× of gestation day 15, day 15 sham treated, and day 15 LPS treated were used. A total of 216 squares per group was manually counted using ImageJ program. A frequency distribution histogram was generated based on the number of fibrils present in each square counted. The number of fibrils was less in day 15 LPS-treated cervices compared to day 15 and day 15 sham-treated cervices, indicating an increased interfibrillar spacing. Note in the graph that there is a shift in the distribution toward a higher number of squares with less of fibrils in the LPS-treated group. n = 3 animals per time point.

decorin [41, 42]. Previous reports have shown that these bridges and their disruption can influence the mechanical integrity of collagen fibrils [43, 44]. Our recent studies demonstrate a key role of decorin in appropriate assembly and mechanical function of collagen fibrils in the nonpregnant cervix, although the requirement for decorin is likely over-ridden by pregnancy-specific compensation by other related proteoglycans [39]. Though the SEM images did not identify any gross malformation of proteoglycan interfibrillar bridges in the LPS group, further molecular analysis of proteoglycans and proteases that may disrupt these bridges is warranted.

Subsequent assessment of collagen I fiber architecture with SHG allowed a global assessment of collagen fiber arrangements in defined regions of the cervix. The LPS-treated cervix exhibited morphological features quantifiably different from untreated and mifepristone-treated cervices. Unlike the mifepristone-treated cervix, which exhibited larger pores uniformly throughout the cervix, the LPS-treated cervix exhibited larger pores restricted to the SE stromal region. This led us to consider whether regional clipping of collagen fibers in the subepithelia may arise from an increased concentration of protease activity derived from immune cells or the cervical epithelia. Neutrophil numbers and expression of matrix metalloprotease 8 (*Mmp8*), a collagenase, are increased in LPS-mediated ripening but not term ripening [7]. In both sterile and infectious tissue damage, increased neutrophil chemotaxis results in formation of neutrophil

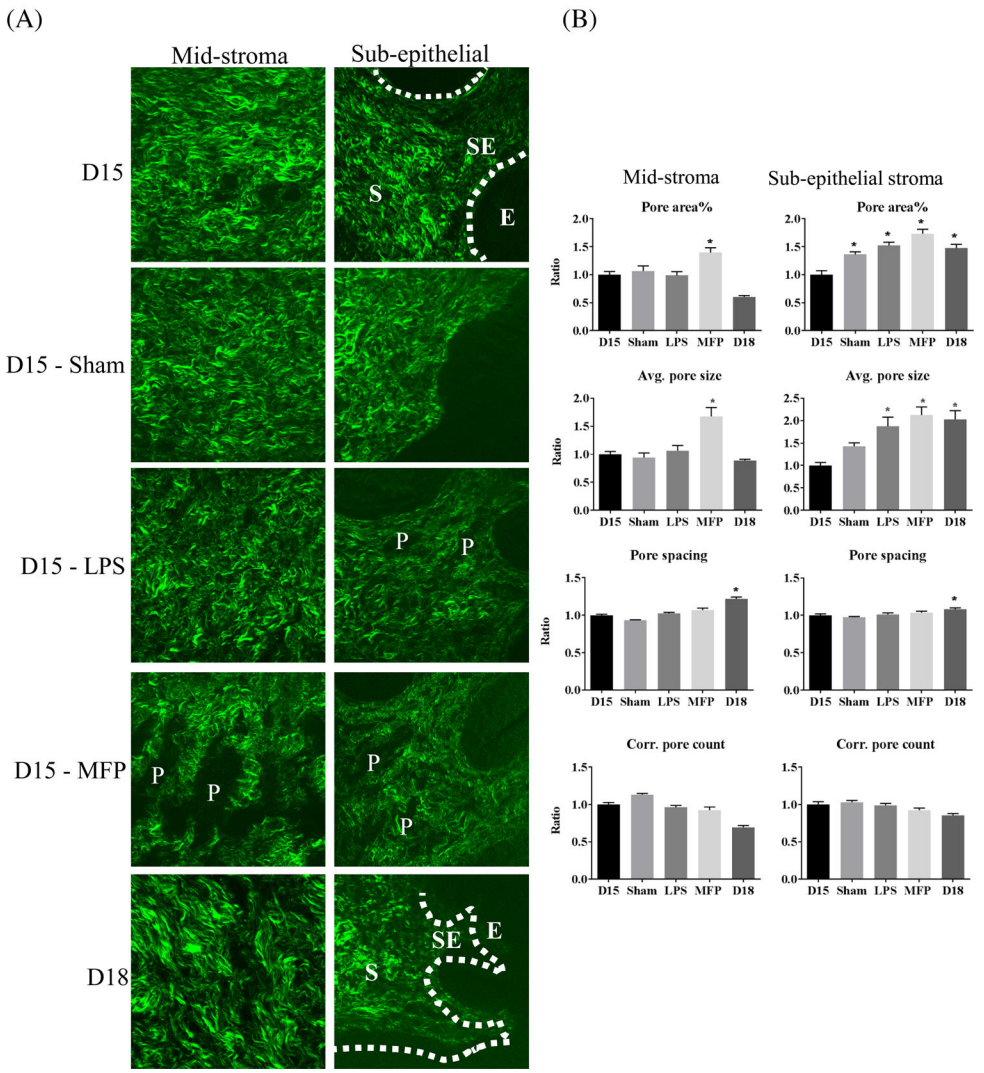

Figure 6. SHG morphological assessment of collagen fiber structure. (A) SHG images of gestation day 15, day 15 sham, day 15 LPS treated, day 15 mifepristone (MFP), treated and day 18 cervical sections. E—epithelium; SE—subepithelial stroma; S—stroma; P—pore. **(B)**. Quantitative image analysis of pores between collagen fibers. In general, 3–4 images were taken from the SE region and MS region per cervical section for SHG. SHG images collected in the forward direction were evaluated for the number of pores, pore size, pore spacing, and pore area %. Pore area % and average pore size increased significantly for mifepristone (MFP)-treated cervices in both MS and SE stromal regions. Pore area % and average pore size increased significantly for LPS-treated cervices only in SE stromal regions. Bars represent the ratio of measurements from images of cross-sections collected throughout the longitudinal extent of the cervix and compared to gestation day 15. Error bars represent standard error of mean ($^*P < 0.05$). n = 3 animals for all time points.

clusters termed neutrophil swarms [37]. These swarms are reported to physically exclude or degrade collagen networks thus allowing an integrin-dependent interaction between neutrophils that may aid to isolate the wound or infectious site from surrounding unaffected tissue [37]. Compared to untreated day 15, there was modest increase in neutrophil cluster size in the sham surgery controls, consistent with this being a model of sterile inflammation. However, the size of clusters, area of occupation, and ability to exclude collagen networks in the LPS-treated group was greater compared to those observed in the cervices of the sham surgery controls. The increased density of protease-rich neutrophils in the SE stroma we suggest contributes to the preferential reorganization of collagen fibers in this region of the cervix. Because the depletion of neutrophils in LPS-treated mice does not prevent LPS-induced PTB [45, 46], we anticipate other immune cells such as macrophages, as well as the cervical epithelial cells may also synthesize and secrete proteases, that impact ECM structure and mechanical function. The presence of proinflammatory and tissue repair macrophages in the cervix at term, postpartum, and in LPS-mediated cervical ripening has been well documented [47–50].

The restricted localization of changes in collagen fiber architecture observed in our mouse model of infection-mediated premature ripening lends further support to current evidence that ECM reorganization near the endocervical canal is the initiating hub critical for mechanical function in term cervical remodeling. This is supported by the observation that one metric of structural organization of collagen—SHG, subepithelial pore area and pore size, is increased in both term and preterm models. In addition, we have previously reported that nonpregnant mice lacking the proteoglycan decorin have abnormal collagen fibrils that resolve during pregnancy starting first in the SE stroma with subsequent resolution in the MS [39]. In NP and pregnant women, assessment of three-dimensional collagen ultrastructure by optical coherence tomography in the cervix identified

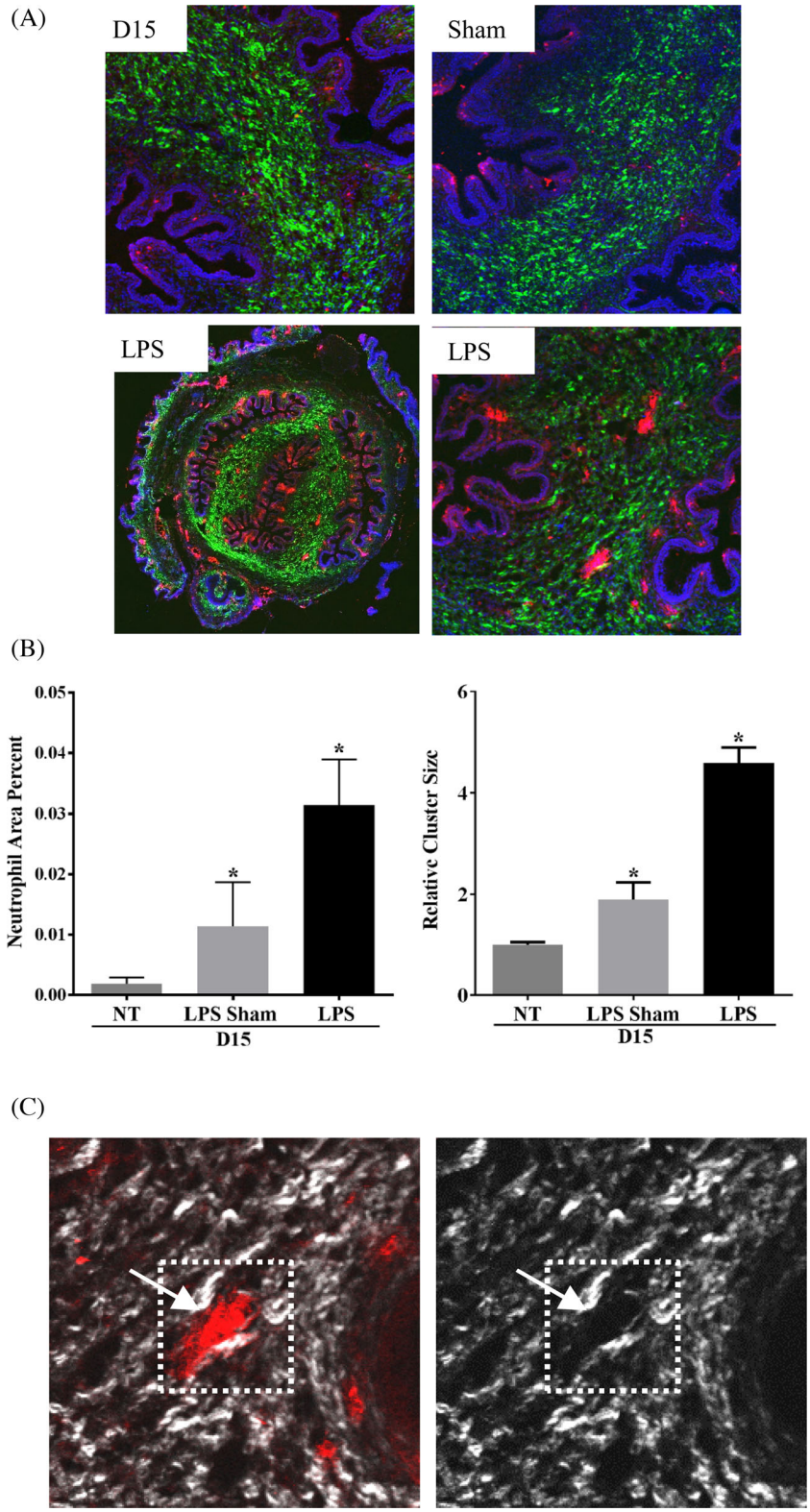

Figure 7. Cervix from LPS-treated mice contains increased neutrophil clusters concentrated in the SE stromal regions. (A) Dual imaging of collagen by SHG (green), neutrophils (red) by IF using the antibody 7/4. High-magnification images in top panel and lower right to day 15, day 15 sham, and day 15 LPS cervices. Lower left panel is a low-magnification tiled image from day 15 LPS. (B) Quantification of neutrophil cluster size and area percent of neutrophils. Both parameters were significantly increased in LPS-treated cervix when compared to day 15 untreated (NT) and day 15 sham cervix (day 15 n = 3, LPS sham n = 2, and LPS n = 5; $^{*}P < 0.05$). (C) Dual SHG (white) and IF—7/4 (red) images. The left panel indicates a neutrophil cluster and the right panel indicates reduced SHG signal in the region with neutrophil cluster.

an increase in collagen fiber disorganization in the pregnant group that included regional variations [51, 52].

Collectively, these findings suggest the diversity of mechanisms by which the cervix can achieve increased compliance and highlight the need for further understanding of the mechanisms by which regional specific ECM reorganization is achieved in term and preterm cervical ripening. While further investigation is required to understand the physiological events that lead to the regionalized changes seen in collagen SHG signal in infection-mediated premature cervical remodeling, these findings support the potential use of the described SHG endoscope [53] or other imaging modalities [54] to identify abnormal cervical collagen structure as a risk factor for PTB.

Supplementary data

Supplementary data are available at *BIOLRE* online.

Supplemental Figure 1. Cross-section of gestation day 18 mouse cervix stained with H&E. The subepithelial stromal region is illustrated with a black box and midstroma region with a blue box. In general, three to four images from each region per cervical section was imaged for SHG or IF microscopy.

Supplementary Figure 2. Tissue sample mounted on Scanning Electron Microscope (SEM) stub. The gestation day 18 cervical sample was processed for scanning electron microscopy as described in methods. The region shown by a yellow square was defined as midstroma and selected for high-magnification imaging as presented in Figure 4.

Supplementary table 1. List of antibodies used.

Acknowledgments

We would like to thank the UTSW Electron Microscopy Core for help with tissue processing and optimization of SEM imaging and sample preparation for TEM and the Live Cell Core Facility for guidance in SHG imaging. We thank Dr Kristin Myers for reading the manuscript and providing suggestions.

Authors' roles:

SN performed mRNA experiments, SHG imaging, and electron microscopy and analyzed the data. MA conducted animal experiments, performed protein analysis, immunofluorescence, SHG imaging, electron microscopy studies, and analyzed the data. BT conducted animal experiments and performed SHG and neutrophil imaging and analyzed the data. KP provided technical support for SHG and electron microcopy imaging. KP and MM guided scientific direction of the project and data analysis. MM, MA, and SN finalized the manuscript. SN, MA, BT, KP, and MM all contributed to manuscript revisions.

Conflict of Interest: The authors have declared that no conflict of interest exists.

References

1. Martin JA, Hamilton BE, Osterman MJ. Births in the United States, 2014. In: *NCHS Data Brief*. U.S. Department of Health and Human Services, USA, 2015:345–354.
2. Blencowe H, Cousens S, Chou D, Oestergaard M, Say L, Moller AB, Kinney M, Lawn J. Born too soon: the global epidemiology of 15 million preterm births. *Am J Obstet Gynecol* 2013; **10**(Suppl 1):S2.
3. Muglia LJ, Katz M. The enigma of spontaneous preterm birth. *N Engl J Med* 2010; **362**:529–535.
4. Romero R, Dey SK, Fisher SJ. Preterm labor: one syndrome, many causes. *Science* 2014; **345**:760–765.
5. Rubens CE, Sadovsky Y, Muglia L, Gravett MG, Lackritz E, Gravett C. Prevention of preterm birth: harnessing science to address the global epidemic. *Sci Transl Med* 2014; **6**:262sr265–262sr265.
6. Gonzalez JM, Xu H, Chai J, Ofori E, Elovitz MA. Preterm and term cervical ripening in CD1 Mice (Mus musculus): similar or divergent molecular mechanisms? *Biol Reprod* 2009; **81**:1226–1232.
7. Holt R, Timmons BC, Akgul Y, Akins ML, Mahendroo M. The molecular mechanisms of cervical ripening differ between term and preterm birth. *Endocrinology* 2011; **152**:1036–1046.
8. Gonzalez JM, Romero R, Girardi G. Comparison of the mechanisms responsible for cervical remodeling in preterm and term labor. *J Reprod Immunol* 2013; **97**:112–119.
9. Mahendroo M. Cervical remodeling in term and preterm birth: insights from an animal model. *Reproduction* 2012; **143**:429–438.
10. Vink J, Feltovich H. Cervical etiology of spontaneous preterm birth. *Semin Fetal Neonatal Med* 2016; **21**:106–112.
11. Rinaldi SF, Makieva S, Frew L, Wade J, Thomson AJW, Moran CM, Norman JE, Stock SJ. Ultrasound-guided intrauterine injection of lipopolysaccharide as a novel model of preterm birth in the mouse. *Am J Pathol* 2015; **185**:1201–1206.
12. Kemp MW, Saito M, Newnham JP, Nitsos I, Okamura K, Kallapur SG. Preterm birth, infection, and inflammation advances from the study of animal models. *Reprod Sci* 2010; **17**:619–628.
13. Bezold KY, Karjalainen MK, Hallman M, Teramo K, Muglia LJ. The genomics of preterm birth: from animal models to human studies. *Genome Med* 2013; **5**:34–34.
14. Elovitz MA, Mrinalini C. Animal models of preterm birth. *Trends Endocrinol Metab* 2004; **15**:479–487.
15. Dudley DJ, Branch DW, Edwin SS, Mitchell MD. Induction of preterm birth in mice by RU486. *Biol Reprod* 1996; **55**:992–995.
16. Yellon SM, Dobyns AE, Beck HL, Kurtzman JT, Garfield RE, Kirby MA. Loss of progesterone receptor-mediated actions induce preterm cellular and structural remodeling of the cervix and premature birth. *PLoS One* 2013; **8**:e81340.
17. Shynlova O, Nedd-Roderique T, Li Y, Dorogin A, Lye SJ. Myometrial immune cells contribute to term parturition, preterm labour and postpartum involution in mice. *J Cell Mol Med* 2013; **17**:90–102.
18. Timmons BC, Reese J, Socrate S, Ehinger N, Paria BC, Milne GL, Akins ML, Auchus RJ, McIntire D, House M, Mahendroo M. Prostaglandins are essential for cervical ripening in LPS-mediated preterm birth but not term or antiprogestin-driven preterm ripening. *Endocrinology* 2014; **155**:287–298.
19. Nott JP, Bonney EA, Pickering JD, Simpson NAB. The structure and function of the cervix during pregnancy. *Transl Res Anat* 2016; **2**:1–7.
20. Singer A, Jordan JA. The functional anatomy of the cervix, the cervical epithelium and the stroma. In: Jordan JA, Singer A (eds.), *The Cervix*. Blackwell Publishing Ltd., Oxford, UK; 2009:13–37.
21. Vink JY, Qin S, Brock CO, Zork NM, Feltovich HM, Chen X, Urie P, Myers KM, Hall TJ, Wapner R, Kitajewski JK, Shawber CJ et al. A new paradigm for the role of smooth muscle cells in the human cervix. *Am J Obstet Gynecol* 2016; **215**:478.e471–478.e411.
22. Timmons B, Akins M, Mahendroo M. Cervical remodeling during pregnancy and parturition. *Trends Endocrinol Metab* 2010; **21**:353–361.
23. Myers KM, Feltovich H, Mazza E, Vink J, Bajka M, Wapner RJ, Hall TJ, House M. The mechanical role of the cervix in pregnancy. *J Biomech* 2015; **48**:1511–1523.
24. Akins ML, Luby-Phelps K, Bank RA, Mahendroo M. Cervical softening during pregnancy: regulated changes in collagen cross-linking and composition of matricellular proteins in the mouse. *Biol Reprod* 2011; **84**:1053–1062.
25. Yoshida K, Jiang H, Kim M, Vink J, Cremers S, Paik D, Wapner R, Mahendroo M, Myers K. Quantitative evaluation of collagen crosslinks and corresponding tensile mechanical properties in mouse cervical tissue during normal pregnancy. *PLoS One* 2014; **9**:e112391.
26. House M, Kaplan DL, Socrate S. Relationships between mechanical properties and extracellular matrix constituents of the cervical stroma during pregnancy. *Semin Perinatol* 2009; **33**:300–307.
27. Bokström H, Norström A. Effects of mifepristone and progesterone on collagen synthesis in the human uterine cervix. *Contraception* 1995; **51**:249–254.

28. Clark K, Ji H, Feltovich H, Janowski J, Carroll C, Chien EK. Mifepristone-induced cervical ripening: structural, biomechanical, and molecular events. *Am J Obstet Gynecol* 2006; **194**:1391–1398.
29. Glassman W, Bryam-Smith M, Garfield RE. Changes in rat cervical collagen during gestation and after antiprogesterone treatment as measured in vivo with light-induced autofluorescence. *Am J Obstet Gynecol* 1995; **173**:1550–1556.
30. Maradny EE, Kanayama N, Halim A, Maehara K, Sumimoto K, Terao T. Effects of neutrophil chemotactic factors on cervical ripening. *Clin Exp Obstet Gynecol* 1995; **22**:76–85.
31. Akins ML, Luby-Phelps K, Mahendroo M. Second harmonic generation imaging as a potential tool for staging pregnancy and predicting preterm birth. *J Biomed Opt* 2010; **15**:026020.
32. Romanic AM, Adachi E, Kadler KE, Hojima Y, Prockop DJ. Copolymerization of pNcollagen III and collagen I. pNcollagen III decreases the rate of incorporation of collagen I into fibrils, the amount of collagen I incorporated, and the diameter of the fibrils formed. *J Biol Chem* 1991; **266**:12703–12709.
33. Liu X, Wu H, Byrne M, Krane S, Jaenisch R. Type III collagen is crucial for collagen I fibrillogenesis and for normal cardiovascular development. *Proc Natl Acad Sci USA* 1997; **94**:1852–1856.
34. Lui PP, Chan LS, Lee YW, Fu SC, Chan KM. Sustained expression of proteoglycans and collagen type III/type I ratio in a calcified tendinopathy model. *Rheumatology* 2010; **49**:231–239.
35. Chen X, Nadiarynkh O, Plotnikov S, Campagnola PJ. Second harmonic generation microscopy for quantitative analysis of collagen fibrillar structure. *Nat Protocols* 2012; **7**:654–669.
36. Campagnola PJ, Loew LM. Second-harmonic imaging microscopy for visualizing biomolecular arrays in cells, tissues and organisms. *Nat Biotechnol* 2003; **21**:1356–1360.
37. Lammermann T, Afonso PV, Angermann BR, Wang JM, Kastenmuller W, Parent CA, Germain RN. Neutrophil swarms require LTB4 and integrins at sites of cell death in vivo. *Nature* 2013; **498**:371–375.
38. Yoshida K, Mahendroo M, Vink J, Wapner R, Myers K. Material properties of mouse cervical tissue in normal gestation. *Acta Biomater* 2016; **36**:195–209.
39. Nallasamy S, Yoshida K, Akins M, Myers K, Iozzo R, Mahendroo M. Steroid hormones are key modulators of tissue mechanical function via regulation of collagen and elastic fibers. *Endocrinology* 2017; **158**:950–962.
40. Nallasamy S, Mahendroo M. Distinct roles of cervical epithelia and stroma in pregnancy and parturition. *Semin Reprod Med* 2017; **35**:190–200.
41. Chen S, Birk DE. The regulatory roles of small leucine-rich proteoglycans in extracellular matrix assembly. *FEBS J* 2013; **280**:2120–2137.
42. Michelacci YM. Collagens and proteoglycans of the corneal extracellular matrix. *Braz J Med Biol Res* 2003; **36**:1037–1046.
43. Panwar P, Du X, Sharma V, Lamour G, Castro M, Li H, Bromme D. Effects of cysteine proteases on the structural and mechanical properties of collagen fibers. *J Biol Chem* 2013; **288**:5940–5950.
44. Liao J, Vesely I. Skewness angle of interfibrillar proteoglycans increases with applied load on mitral valve chordae tendineae. *J Biomech* 2007; **40**:390–398.
45. Rinaldi SF, Catalano RD, Wade J, Rossi AG, Norman JE. Decidual neutrophil infiltration is not required for preterm birth in a mouse model of infection-induced preterm labor. *J Immunol* 2014; **192**:2315–2325.
46. Filipovich Y, Agrawal V, Crawford SE, Fitchev P, Qu X, Klein J, Hirsch E. Depletion of polymorphonuclear leukocytes has no effect on preterm delivery in a mouse model of Escherichia coli-induced labor. *Am J Obstet Gynecol* 2015; **213**:697.e691–610.
47. Timmons BC, Fairhurst AM, Mahendroo MS. Temporal changes in myeloid cells in the cervix during pregnancy and parturition. *J Immunol* 2009; **182**:2700–2707.
48. Payne KJ, Clyde LA, Weldon AJ, Milford TA, Yellon SM. Residency and activation of myeloid cells during remodeling of the prepartum murine cervix. *Biol Reprod* 2012; **87**:106.
49. Gonzalez JM, Dong Z, Romero R, Girardi G. Cervical remodeling/ripening at term and preterm delivery: the same mechanism initiated by different mediators and different effector cells. *PLoS One* 2011; **6**:e26877.
50. Gonzalez JM, Franzke CW, Yang F, Romero R, Girardi G. Complement activation triggers metalloproteinases release inducing cervical remodeling and preterm birth in mice. *Am J Pathol* 2011; **179**:838–849.
51. Gan Y, Yao W, Myers KM, Vink JY, Wapner RJ, Hendon CP. Analyzing three-dimensional ultrastructure of human cervical tissue using optical coherence tomography. *Biomed Opt Express* 2015; **6**:1090–1108.
52. Yao W, Gan Y, Myers KM, Vink JY, Wapner RJ, Hendon CP. Collagen fiber orientation and dispersion in the upper cervix of non-pregnant and pregnant women. *PLoS One* 2016; **11**:e0166709.
53. Zhang Y, Akins ML, Murari K, Xi J, Li MJ, Luby-Phelps K, Mahendroo M, Li X. A compact fiber-optic SHG scanning endomicroscope and its application to visualize cervical remodeling during pregnancy. *Proc Natl Acad Sci USA* 2012; **109**:12878–12883.
54. Feltovich H, Hall TJ, Berghella V. Beyond cervical length: emerging technologies for assessing the pregnant cervix. *Am J Obstet Gynecol* 2012; **207**:345–354.